Cousins at work: How combining medical with optical imaging enhances *in vivo* cell tracking.

Alessia Volpe[1], Ewelina Kurtys[1], Gilbert O. Fruhwirth[1,*].

[1] Department of Imaging Chemistry and Biology, School of Biomedical Engineering and Imaging Sciences, King's College London, SE1 7EH, London, UK.

Correspondence to:
Dr Gilbert Fruhwirth, Department of Imaging Chemistry and Biology, School of Biomedical Engineering and Imaging Sciences, King's College London, St. Thomas' Hospital, Lambeth Wing 4th floor, SE1 7EH, London, UK; e-mail: gilbert.fruhwirth@kcl.ac.uk.

Abstract

Microscopy and medical imaging are related in their exploitation of electromagnetic waves, but were developed to satisfy differing needs, namely to observe small objects or to look inside subjects/objects, respectively. Together, these techniques can help elucidate complex biological processes and better understand health and disease. A current major challenge is to delineate mechanisms governing cell migration and tissue invasion in organismal development, the immune system and in human diseases such as cancer where the spatiotemporal tracking of small cell numbers in live animal models is extremely challenging.

Multi-modal multi-scale *in vivo* cell tracking integrates medical and optical imaging. Fuelled by basic research in cancer biology and cell-based therapeutics, it has been enabled by technological advances providing enhanced resolution, sensitivity and multiplexing capabilities. Here, we review which imaging modalities have been successfully used for *in vivo* cell tracking and how this challenging task has benefitted from combining macroscopic with microscopic techniques.

Keywords

Cancer metastasis / cell therapy / microscopy / reporter genes / whole-body imaging.

Introduction

Two major discoveries, one enabling observation of smaller objects and the other allowing to look inside subjects/objects, significantly boosted biological/biomedical research. The first compound microscope was invented by Hans and Zaccharias Jansen in the late 16th century, which triggered later microscopy development that in turn enabled the direct observation of atoms, single molecules and single-/multi-cellular organisms including their dynamics. The second transformation was Wilhelm Roentgen's discovery of X-rays in 1895, which enabled investigations of inner subject/object structures in a non-invasive way (genetic effects of radiation were only recognized later) and founded medical imaging. Both microscopy and medical imaging rely on the interaction of biological matter with electromagnetic waves, but medical imaging employs a wider range than microscopy including α/β/γ-ray-emitting radioisotopes, X-rays, visible (VIS)/near-infrared (NIR) light, radio waves and ultrasound (Fig.1). Medical imaging revolutionized the diagnosis and treatment of human disease by providing anatomical, physiological and molecular information (Mankoff, 2007). Imaging modalities differ in their capabilities and limitations (Fig.1), hence combination technologies were introduced to exploit them best ('multi-modal imaging'). For example, positron emission tomography (PET) offers best-in-class sensitivity and absolute quantification but only at millimetre resolution and was combined with modalities providing higher resolution such as computed tomography (CT) (Basu et al., 2014) or magnetic resonance imaging (MRI) (Catana, 2017). How medical imaging can be used to develop biomarkers providing diagnostic, prognostic, predictive, and treatment monitoring information was recently standardized (O'Connor et al., 2017). Photoacoustic tomography (PAT) and Cerenkov luminescence imaging (CLI) are special in that they both rely on electromagnetic waves from different parts of the spectrum for imaging. PAT delivers NIR laser pulses into biological tissues with the latter absorbing and converting some of the laser pulse energy into heat, leading to transient thermoelastic expansion and thus wideband ultrasonic emission (Ntziachristos et al., 2005;Wang and Yao, 2016). CLI relies on the collection of light produced by charged particles traversing through biological tissue with a velocity greater than the phase velocity of light in that medium (Ciarrocchi and Belcari, 2017). Brightfield microscopy and, less frequently, fluorescence microscopy are routine techniques providing confirmatory pathology information obtained from biopsied tissues. Recently, automated multiplex fluorescence histopathology (Mansfield et al., 2008;Stack et al., 2014) has enabled rigorous tissue profiling, *e.g.* immune infiltration in tumour tissues (Galon et al., 2014).

Here, we review which imaging modalities have been successfully used for *in vivo* cell tracking and how this challenging task benefitted from combining macroscopic with microscopic techniques. For detailed information on the instrumentation of individual imaging technologies and their use, we provide references to recent specialist literature.

The need for *in vivo* cell tracking in cancer research

A major challenge in cancer research is to better understand the mechanisms governing cell migration and tissue invasion. A plethora of different models including animal tumour models are used for this purpose. It remains extremely challenging to reliably quantify the *in vivo* distribution, relocalisation, and viability of cancer cells in animal tumour models, which are sufficiently large to be optically opaque. For example, the spatiotemporal quantification of cancer cell spread in mouse models of metastasis is a needle-in-a-haystack task. Traditionally, in preclinical cancer research one target organ of metastasis was chosen, large animal cohorts were sacrificed at different time points to overcome inter-animal variability and these approaches were paired with microscopic or flow cytometric analyses in target tissues as read-outs. Whole-body imaging can (i) inform on *in vivo* cell distribution, for example, visualize unexpected metastatic sites; (ii) provide quantitative data, *e.g.* live tumour volumes/metastatic burden and extent of cell therapy on-site residence over time; (iii) provide cell viability data; (iv) reduce inter-subject variability as serial imaging of the same subjects provides statistically better paired data; and (v) can minimize animal usage during preclinical development. Similarly, when developing anti-cancer drugs, it is important to establish targeting efficiency, pharmacokinetics and pharmacodynamics, whether there is spatial heterogeneity to the delivery, and if drug presence is related to therapeutic efficacy. Again, this can be achieved by combining preclinical whole-body cancer cell tracking with conventional molecular imaging of drugs, for example, by image-based quantification of the extent a labelled drug reaches *in vivo* traceable cancer cells and whether the drug is delivered to all primary/secondary lesions.

Another area where *in vivo* cell tracking is an emerging valuable tool is the development and clinical translation of cell-based therapies. Unlike conventional chemotherapeutics or targeted therapies, they cannot be considered as 'fire-and-forget' weapons in the battle against cancer as they are live cell products, but little is known about their *in vivo* distribution and fate both preclinically and clinically. In 2017, the FDA approved the first clinical products, tisagenlecleucel and axicabtagene ciloleucel, which are autologous CD19b-targeted chimeric antigen receptor T-cell (CAR-T) immunotherapies for the treatment of certain blood cancers (B-cell lymphomas; (USFood&DrugAdministration, 2017a;b)). CAR-T immunotherapies have the potential to be curative, but not all patients respond and sometimes the effects are only temporary (Maude et al., 2018;Neelapu et al., 2017;Schuster et al., 2017). CAR-T are also associated with severe/life-threatening side-effects and fatalities during trials (Linette et al., 2013;Saudemont et al., 2018). Moreover, cellular immunotherapeutics for treating solid tumours are at the clinical trial stages but not yet routinely available to patients. Traditional approaches in preclinical cell therapy development rely on dose escalation with toxicity evaluation, tumorigenicity tests, and qPCR-based persistence determination. However, clinical trials are still performed without knowledge about the *in vivo* distribution and fate of the administered therapeutic cells, making it impossible to adequately monitor and assess their safety. Major unresolved questions in cell therapy

development and use both preclinically and clinically are: (i) the whole-body distribution of therapeutic cells; (ii) their potential for re-location during treatment and the kinetics of this process; (iii) whether on-target off-site toxicities occur; (iv) how long the administered cells survive; and (v) which biomarkers are best suited to predict and monitor cell therapy efficacy. Whole-body imaging-based *in vivo* cell tracking can inform on many of these aspects in a truly non-invasive manner.

Rendering cells traceable *in vivo*

In vivo cell tracking exploits molecular imaging mechanisms but differs from conventional molecular imaging as contrast agents or contrast-forming features are added to the cells before their administration into subjects. On some occasions, features that can be exploited for generating contrast are intrinsic, for example, when cancer cells express molecules that show low or no expression in other tissues. Under these circumstances conventional molecular imaging offers tracking possibilities both preclinically and clinically (*e.g.* sodium iodide symporter (NIS) in thyroid metastases (Kogai and Brent, 2012;Portulano et al., 2014), glutamate carboxypeptidase 2 (PSMA) in prostate cancer (Oliveira et al., 2017;Perera et al., 2016), carcinoembryonic antigen in colorectal cancer (Tiernan et al., 2013), or melanin in melanomas (Tsao et al., 2012)). However, in most cases contrast agents or contrast-forming features must be introduced to the cells of interest, and, crucially, this must be done with the experimental design in mind (technology, tracking time, tracking interval, preclinical/clinical setting).

Labels can be introduced into cells via two fundamentally different methodologies. So-called 'direct cell labelling' employs ready-to-use contrast agents (*e.g.* organic fluorophores, quantum dots, iron oxide nanoparticles, F-19-fluorinated contrast agents, chelated radiometals etc.), which are introduced into cells either due to the contrast agents being cell permeant, or through assisted uptake (*e.g.* by transfection or internalisation) (Kircher et al., 2011). The alternative is 'indirect cell labelling', whereby a genetically encoded reporter is ectopically introduced to the cells mostly by viral transduction to ensure genomic integration and long-term expression. In some cases, episomal plasmids (*e.g.* delivered using transfection or electroporation to deliver the DNA) can also be useful. Lately, gene editing approaches have been reported for reporter insertion, which are have advantages over viral transduction as they offer precise control over the genomic site of reporter insertion (Bressan et al., 2017). Contrast formation relies on either (a) label uptake by reporters that are transporters, (b) label binding to cell surface-expressed reporters, or (c) expression of contrast-forming proteins (*e.g.* fluorescent proteins, luciferases). All these indirect mechanisms find utility in reporter gene applications, which are used to image intracellular molecular events or, as discussed here, to perform *in vivo* cell tracking.

Reporter genes (Tab.1) have critical advantages over direct labelling for cell tracking. First, the observation period is independent of the contrast agent, for example, not affected by the half-lives of a radioisotope. Second, genetic encoding avoids label dilution phenomena, which are

particularly limiting observation times in the case of fast growing cells (*e.g.* cancer cells or expanding T cells). Third, genetic encoding circumvents complex cell labelling procedures and potential associated cell damage/toxicities. A drawback of the indirect cell labelling approach is that it requires genetic engineering. However, this is neither a concern for preclinical experimentation nor for cell therapies already reliant on it (*e.g.* CAR-T) (Saudemont, Jespers, 2018). A caveat exists in the potential for immune system activity against reporters as cells expressing foreign reporters can be detected, attacked, and cleared by an intact immune system. This may best be overcome by using host reporter proteins that are normally endogenously expressed in the organism of interest. Importantly, these host reporters should be endogenously expressed in only a limited number of host tissues, to exclude interference with the experimental goals, and ideally at low levels to ensure favourable contrast.

Optical imaging – versatility and limitations

Selecting technology for the task of *in vivo* cell tracking is not a straightforward task. The group of optical imaging technologies overall offers the widest versatility across multiple length scales, spanning microscopy and macroscopic medical imaging (Fig.1). Fluorescence is the only imaging modality capable to bridge the length scales (macroscopic, (sub)cellular, molecular), hence would appear most attractive for the task of *in vivo* cell tracking. For example, using one fluorescent dye, whole-body imaging and tissue microscopy data were acquired (Swirski et al., 2007). However, no single optical approach can cover all requirements for *in vivo* cell tracking despite recent technological advancements. For example, improvements in fluorescence microscopy have allowed deeper sample penetration and imaging larger specimen (*cf.* light sheet and expansion microscopy, tissue clearing (Ariel, 2017;Karagiannis and Boyden, 2018;Whitehead et al., 2017)). Moreover, intravital fluorescence microscopy offers cellular resolution in live animals, but only in very limited fields of view and in certain accessible tissues (Alieva et al., 2014;Condeelis and Segall, 2003;Entenberg et al., 2017;Entenberg et al., 2018;Pittet and Weissleder, 2011). In contrast, both fluorescence and bioluminescence whole-body imaging (BLI and FRI/FLI) offer large fields of views but suffer from poor resolution (Fig.1) that is insufficient for *in vivo* cell tracking and are planar imaging technologies and thus unable to provide 3D or quantitative data. BLI offers orders of magnitude better sensitivities than all macroscopic fluorescence techniques and is inexpensive but requires the tissue availability of a luminescence substrate, is limited in its multiplexing capability, and confined to preclinical use (Dunlap, 2014;Jiang et al., 2016;Li et al., 2013). To obtain true 3D data a tomographic design is required. This is provided by optical projection tomography (OPT), which can be considered to be the optical analogue of X-ray computed tomography (CT). OPT operates on the micrometre to millimetre scales (Cheddad et al., 2012;Sharpe et al., 2002) thereby bridging the scale gap between BLI/FLI and microscopy. It can either provide tomographic data on light absorption or fluorescence signals, and has been used in

live zebrafish (Bassi et al., 2011;McGinty et al., 2011), fruit flies (Arranz et al., 2014;Vinegoni et al., 2008) and for whole organ imaging in mice (Alanentalo et al., 2008;Gleave et al., 2012;Gupta et al., 2013). An alternative approach offering larger fields of view in the centimetre range is diffuse optical tomography or fluorescence mediated tomography (FMT), which exploits photon tissue propagation theory to allow for 3D reconstruction at centimetre depth but its resolution is hampered by weak signals and high scattering (Fig.1; (Graves et al., 2004;Lian et al., 2017;Ntziachristos, 2006;Venugopal et al., 2010;Wang et al., 2015;Zacharakis et al., 2011)). The group of photoacoustic techniques including PAT (Dean-Ben et al., 2017;Valluru et al., 2016;Wang and Yao, 2016) and its more refined variants multispectral optoacoustic tomography (MSOT; (Ma et al., 2009;Ntziachristos and Razansky, 2010)) and raster scanning optoacoustic mesoscopy (RSOM; (Omar et al., 2015)) are the newest additions to the optical imaging portfolio. They are special in that light is only used for excitation while sound is what is recorded, thereby rendering them less affected by the shortcomings of using light for imaging thick samples. However, it is important to realize that fundamentally all optical whole-body imaging techniques are severely affected by differential light absorption, scatter and poor depth penetration, precluding full 3D quantification (Fig.1). Hence, they play a minor role in medical imaging, albeit with a few notable exceptions although outside the field of cell tracking. First, optical coherence tomography (OCT) in ophthalmology (Jung et al., 2011;Tao et al., 2013) and dermatology (Mogensen et al., 2009;Olsen et al., 2015), and, second, photoacoustic imaging as a promising emerging tool in oncology and for the assessment of Crohn's disease (Diot et al., 2017;Knieling et al., 2017;McNally et al., 2016;Valluru, Wilson, 2016). In summary, despite the combined imaging opportunities provided by the various optical approaches, currently, there is no suitable route for reliable *in vivo* cell tracking available, which requires high sensitivity at good resolution within large fields of view while also providing anatomical context.

Multi-modal imaging is necessary for *in vivo* cell tracking

For successful *in vivo* cell tracking, it is necessary to build on the strengths of different imaging modalities and combine them with microscopy. CT and MRI both offer anatomical reference, whereby MRI excels in soft-tissue contrast and avoids the use of ionising radiation but is more expensive. The exquisite sensitivity of BLI has been frequently exploited in combination with MRI, *e.g.* for imaging tumour growth or treatment response in preclinical models (Jost et al., 2009;McCann et al., 2009). In animal models, cell tracking by MRI using, for example, iron oxide nanoparticles has been reported, but cross-correlation studies with luciferase/BLI have demonstrated its shortcomings in sensitivity (Song et al., 2009;Zhang et al., 2011). Dual-contrast agents for ^{19}F-MRI and fluorescence, *e.g.* perfluorocarbon-TexasRed, have been used to track tumour-associated macrophages in mice (Makela and Foster, 2018). MRI reporter genes have also been developed (Tab.1) and have the advantage of co-registration with soft-tissue anatomy and

certain functional imaging parameters. However, MRI sensitivity remains poor compared to BLI and radionuclide imaging (Fig.1). While fluorescent proteins and luciferases are excellent reporters, which also offer multiplexing capability (Mezzanotte et al., 2017;Rodriguez et al., 2017), they suffer from the limitations of optical imaging (see above). In contrast, radionuclide imaging (PET, SPECT) offers best depth penetration and absolute quantification (Lajtos et al., 2014) with preclinical resolutions ≤1 mm (Deleye et al., 2013;Nagy et al., 2013), but radionuclide imaging is more complex to perform and cell detection sensitivities are highly reporter-dependent and cell-specific. Cellular detection sensitivities have been reported to be as good as hundreds/thousands for cancer cells using NIS together with its PET and SPECT radiotracers, respectively, (Diocou et al., 2017;Fruhwirth et al., 2014) and tens of thousands for smaller T-cells using various different reporters in preclinical experiments (Moroz et al., 2015). As PET-CT/MRI and SPECT-CT/MRI instruments are nowadays preclinical and clinical standard, these multimodal approaches offer high sensitivities via PET or SPECT combined with CT or MRI, which add anatomical reference at higher resolution than radionuclide imaging techniques (Fig.1). CLI is unlikely to play a role in *in vivo* cell tracking as it is less sensitive as compared to PET/SPECT and suffering from the shortcomings of optical imaging at depth (see above). Importantly, fluorescence is an excellent partner to complement radionuclide imaging as it excels in the microscopic domain enabling spatial identification of fluorescent cells in tissues (*ex vivo* in tissues or *in vivo* if combined with intravital imaging of specific regions of interest). An additional practical aspect is that genetically encoded fluorescent reporters can be used as selection markers during generation and characterization of radionuclide/fluorescence dual-mode reporter-expressing cells.

Multi-scale *in vivo* cell tracking in practice

Multi-modal multi-scale imaging has enabled quantitative *in vivo* tracking of tumour growth and spontaneous metastasis in preclinical models. SPECT/CT and PET/CT were used to determine location, organ selectivity and extent of metastasis, while fluorescence streamlined cell line generation and characterization, guided dissection, and enabled straightforward fluorescence histology (Fig.2) (Diocou, Volpe, 2017;Fruhwirth, Diocou, 2014;Hekman et al., 2017;Minn et al., 2005;Ray et al., 2004;Volpe et al., 2018). Various radionuclide reporters have been used including those offering options to kill administered cells (*e.g.* HSV1-*tk* (Kokoris and Black, 2002;Ponomarev et al., 2004), deoxycytidine kinases (dCK) (Lee et al., 2017;Likar et al., 2010)). Another reporter, NIS, has a long history (Carlson et al., 2009;Che et al., 2005;Dingli et al., 2006;Groot-Wassink et al., 2004;Higuchi et al., 2009;Merron et al., 2007;Sieger et al., 2003;Terrovitis et al., 2008) and excels in cell tracking because it accurately reports cell viability as transport relies on an intact Na^+/K^+-gradient (Dohan et al., 2003;Portulano, Paroder-Belenitsky, 2014). The NIS-fluorescent protein fusion reporter (NIS-FP) (Fruhwirth, Diocou, 2014;Volpe, Man, 2018) offers direct

accessibility of its subcellular localization (a prerequisite for NIS tracer transport/imaging) at all experimental stages and aids histological tissue segmentation.

This approach also enabled imaging how drugs affect tumour progression/metastasis in animal models. For example, etoposide was found to not abrogate spontaneous metastasis in a preclinical model of breast cancer. Metabolic molecular imaging using [^{18}F]FDG-PET showed etoposide efficacy in cancer tissues due to etoposide-mediated glucose transporter down-modulation (Witney et al., 2009). But it was NIS-FP that, unaffected by etoposide, enabled quantification of tumour progression in different microenvironments (using serial dual-isotope PET/SPECT/CT imaging). NIS-FP also significantly streamlined the *ex vivo* analysis of etoposide effects on reporter expressing cancer cells (Fruhwirth, Diocou, 2014). Other preclinical radionuclide-fluorescence studies employed, for example, dCK/GFP to investigate tumour growth and T-cell trafficking (Likar, Zurita, 2010), or used SPECT-traceable neural stem cells for glioma targeting (Cheng et al., 2016).

Multiplex imaging also enabled differential tracking of molecular and cellular therapeutics to cancer tissues in animal models. In luciferase-expressing non-small cell lung cancers gadolinium- and Cy5.5-labelled nanoparticles were evaluated as potential orotracheally administered tumour diagnostics. Tumour cell tracking relied on BLI while MRI visualized the diagnostic agent and provided anatomical reference, and fluorescence streamlined histological confirmation (Bianchi et al., 2014). Combined serial PET/SPECT/CT-fluorescence imaging also enabled tracking of radiolabelled liposomal mevalonate pathway inhibitors to NIS-FP-expressing tumours and metastases (Fig.3). This study demonstrated the need for a longer interval between administration of this γδ T-cell therapy booster (Lavoue et al., 2012;Mattarollo et al., 2007;Parente-Pereira et al., 2014) and the corresponding γδ T-cell therapy (Edmonds et al., 2016). Conventional reporter gene-based tracking of adoptive cell therapies has also been performed (Koya et al., 2010;Likar, Zurita, 2010;Moroz, Zhang, 2015). The full potential of co-tracking the cell therapy to the tumour was unlocked only very recently; by co-tracking PET-traceable γδ T-cells to NIS-FP-traceable cancer cells in an animal model of human breast cancer, demonstrating that liposomal alendronate pre-treatment caused higher tumour uptake of γδ T-cells (Man et al., 2017). Notably, also as a proof-of-principle study in human glioma patients has recently been performed, employing PET for intra-organ administered CAR-T tracking with MRI providing anatomical context (Keu, Witney, 2017).

Conclusion and outlook

Multi-modal multi-scale *in vivo* cell tracking is a rapidly growing interdisciplinary area, which has been fuelled by the rise of cell-based therapies and enabled by recent technological advances providing enhanced resolution, sensitivity and multiplexing capabilities on both the macroscopic and microscopic scales. For long-term *in vivo* cancer cell tracking, reporter gene methodologies are particularly attractive. The most promising methodologies to-date exploit the exquisite

sensitivity, multiplex capability and 3D quantification of radionuclide imaging and combine them with fluorescence methodologies, thereby allowing convenient cell line generation and reliable and versatile *ex vivo* microscopic analyses. *In vivo* cell tracking cannot always be directly translated for human use because fluorescent proteins, luciferases and certain non-human radionuclide reporters have no direct clinical utility. But importantly, preclinical *in vivo* cell tracking serves as a versatile platform for understanding the underlying biology and to validate therapeutic concepts, thereby informing subsequent clinical trials. However, in the case of live cell therapies, *in vivo* cell tracking provides the means for long-term monitoring in patients if required. It is noteworthy that cell therapies are emerging also in other fields than cancer including transplantation immunology (Boardman et al., 2017) and regenerative medicine (Ellison et al., 2013;Rashid et al., 2015). Multi-modal multi-scale *in vivo* imaging-afforded cell tracking is therefore likely to become increasingly important for the successful development of such cell therapies, particularly in the context of therapy safety and monitoring.

Abbreviations

BLI: bioluminescence imaging; CEST: Chemical exchange saturation transfer; CLI: Cerenkov luminescence imaging; CM: confocal fluorescence microscopy; CT: X-ray computed tomography; FLI/FRI: fluorescence imaging/fluorescence reflectance imaging; FMT: fluorescence mediated tomography; HF: high-frequency; IVM: intravital microscopy; MRI: magnetic resonance imaging; MSOT: multispectral optoacoustic tomography; NIR: near-infrared spectrum; OCT: optical coherence tomography; OPT: optical projection tomography; PAT: photoacoustic tomography; RSOM: high-resolution raster scanning optoacoustic mesoscopy; PET: positron emission tomography; SPECT: single photon computed emission tomography; SRM: super-resolution microscopy (a group of various technologies including but not limited to photoactivated localisation microscopy (PALM), various stochastic optical reconstruction microscopy (STORM) techniques, stimulated emission depletion microscopy (STED), and ground state depletion individual molecule return (GSDIM)); TPM: tow-photon excitation microscopy; US: ultrasound imaging including Doppler and high-frequency ultrasound techniques; VIS: visible light spectrum.

Acknowledgements

We would like to thank Dr Jeremy Carlton (King's College London and The Francis Crick Institute) for his very helpful suggestions in editing the manuscript. The authors receive support from Cancer Research UK via a Multidisciplinary Project Award [C48390/A21153] to GOF supporting AV, and a Worldwide Cancer Research grant [16-1135] to GOF supporting EK. Further they are supported by the King's College London and UCL Comprehensive Cancer Imaging Centre, funded by Cancer Research UK and EPSRC; the National Institute for Health Research (NIHR) Biomedical Research Centre based at Guy's and St Thomas' NHS Foundation Trust and King's College London; and the Wellcome/EPSRC Centre for Medical Engineering at King's College London [WT 203148/Z/16/Z]. The views expressed are those of the authors and not necessarily those of the NHS, the NIHR, or the DoH.

Disclosures

The authors declare that they have no competing financial interests.

Modality	Energy	Spatial resolution / Field of view	Imaging depth	Sensitivity	Multichannel	Cost
PET	γ-rays**			pM	no	$$$
SPECT	γ-rays			pM	≤3	$$$
CT	X-rays			***	no	$
BLI	VIS			fM-pM	2	$
SRM	VIS			single molecule	multiple	$$$
CM	VIS /(NIR)			*	multiple	$
IVM	VIS/NIR			*	multiple	$$
TPM	VIS/NIR			*	multiple	$$
FLI/FRI	(VIS)/NIR			(pM)-nM	multiple	$
FMT	NIR			(pM)-nM	multiple	$$
OCT	NIR			****	multiple	$
OPT	NIR			*	multiple	$
PAT/MSOT	NIR/sound			10nM-uM	multiple	$$
RSOM	NIR/sound			10nM-uM	multiple	$
MRI	Radiowaves			10uM-mM	no[&]	$$$
US	HF sound			*****	no	$

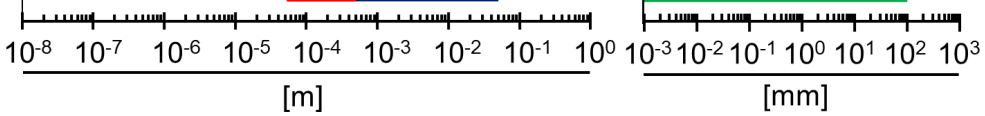

Figure 1. Macroscopic and microscopic imaging modalities | Imaging modalities are ordered according to the electromagnetic spectrum they exploit for imaging (top: high energy; bottom: low energy). Routinely achievable spatial resolution (left end) and fields of view (right end) are shown in red. Where bars are blue they overlap red bars and indicate the same parameters but achievable with instruments used routinely in the clinic. Imaging depth is shown in green alongside sensitivity ranges. Instrument cost estimations are classified as ($) <125,000 $, ($$) 125-300,000 $ and ($$$) >300,000 $. * Fluorophore detection can suffer from photobleaching by excitation light. ** Generated by positron annihilation (511keV). *** Contrast agents sometimes used to obtain different anatomical/functional information. **** In 'emission mode' comparable to other fluorescence modalities (~nM). ***** Highly dependent on contrast agent. [&] Multichannel MRI imaging has been shown to be feasible (Zabow et al., 2008).

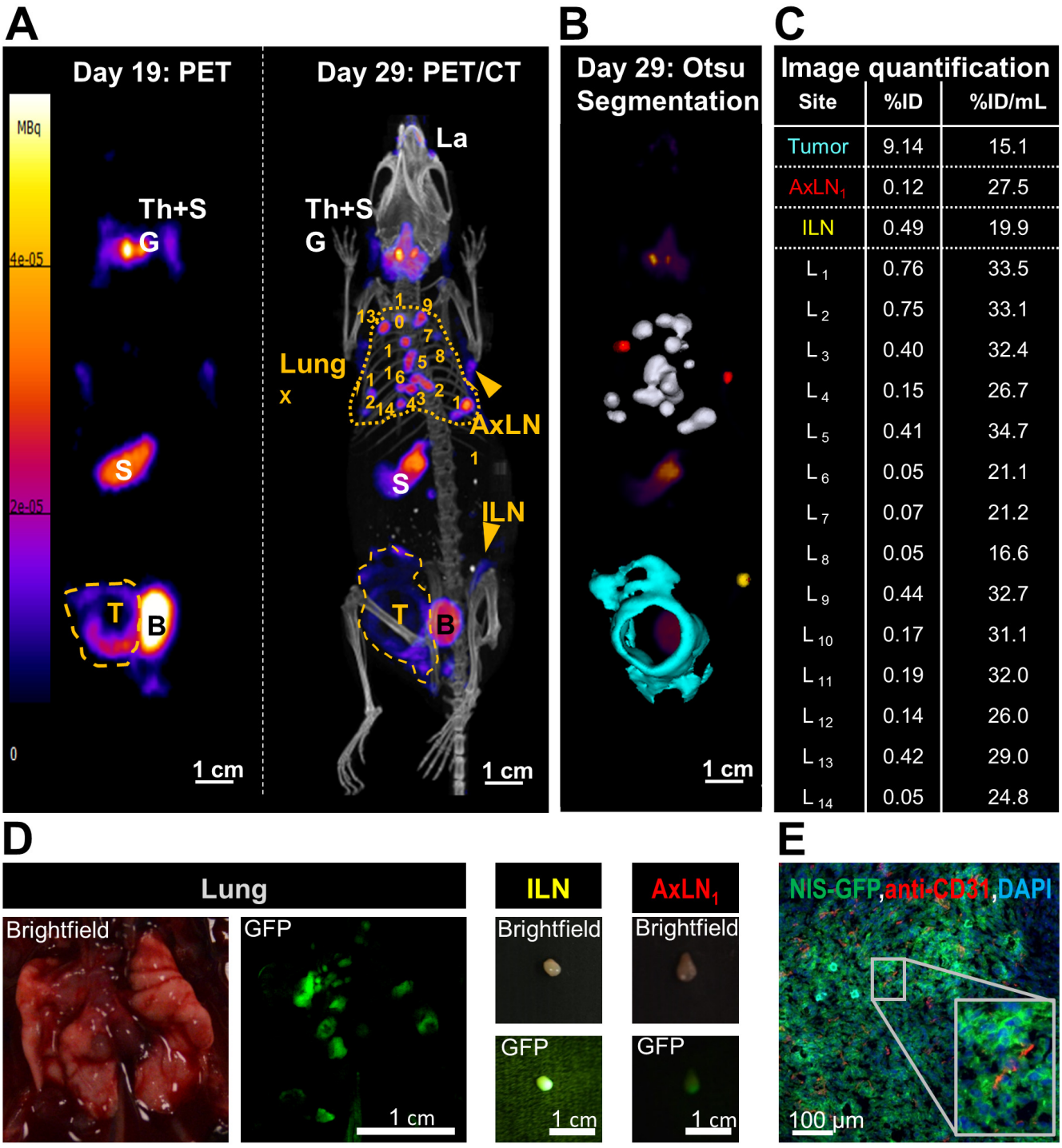

Figure 2. Dual-mode radionuclide-fluorescence metastasis tracking is quantitative and provides data across multiple length scales | Representative results of metastasis tracking in a murine model of inflammatory breast cancer using the radionuclide-fluorescence fusion reporter NIS-GFP are shown. NIS served as an *in vivo* reporter and was imaged by PET/CT using the NIS tracer [^{18}F]BF_4^-. **(A/left)** On day 19 post tumour inoculation, the primary tumour (yellow dashed line) was clearly identified but no metastasis. It is noteworthy that endogenous NIS signals (white descriptors) were also recorded, *i.e.* the thyroid and salivary glands (Th+SG), the stomach (S), and, at very low levels, some parts of the mammary and lachrymal glands. Neither of these endogenous signals interfered with sites of expected metastasis in this tumour model. The bladder (B) signal stems from tracer excretion. **(A/right)** On day 29 post tumour inoculation, metastases were clearly identified in the lung (yellow dotted line; numbered individual metastases) and in some lymph nodes (inguinal (ILN), axillary (AxLN); yellow arrowheads). The primary tumour (yellow dashed line) had also invaded into the peritoneal wall. Images presented are maximum intensity projections (MIP). **(B)** A 3D implementation of the Otsu thresholding technique enabled 3D surface rendering of cancerous tissues; these are superimposed onto a PET MIP. Lung metastases are shown in white, metastatic axillary lymph nodes in red, the metastatic inguinal lymph node in yellow, and the primary tumour that invaded into the peritoneal wall in turquoise. **(C)** Radiotracer uptake into cancerous tissues was quantified from 3D images (%injected dose (ID)) and normalized by the corresponding volumes (%ID/mL). Individual lung metastases correspond to the numbers in (A). **(D)** NIS-GFP's fluorescence properties guided animal dissection. As exemplars brightfield and fluorescence images of the lung with several metastatic lesions and two positive lymph nodes are shown. **(E)** Immunofluorescence histology of the primary tumour. NIS-GFP expressing cancer cells were directly identified without the need for antibody staining. Blood vessels were stained with a rabbit antibody against mouse PECAM-1/CD31 and for nuclei (DAPI) before being imaged by confocal fluorescence microscopy. Data demonstrated vascularization heterogeneity of the primary tumour. The image also shows that the NIS-GFP reporter predominantly resides in the plasma membranes of the tumour cells demonstrating its correct localization to be functional *in vivo* and enabling tumour cell segmentation.

[The figure is reproduced with permission and minor rearrangements from (Volpe, Man, 2018)].

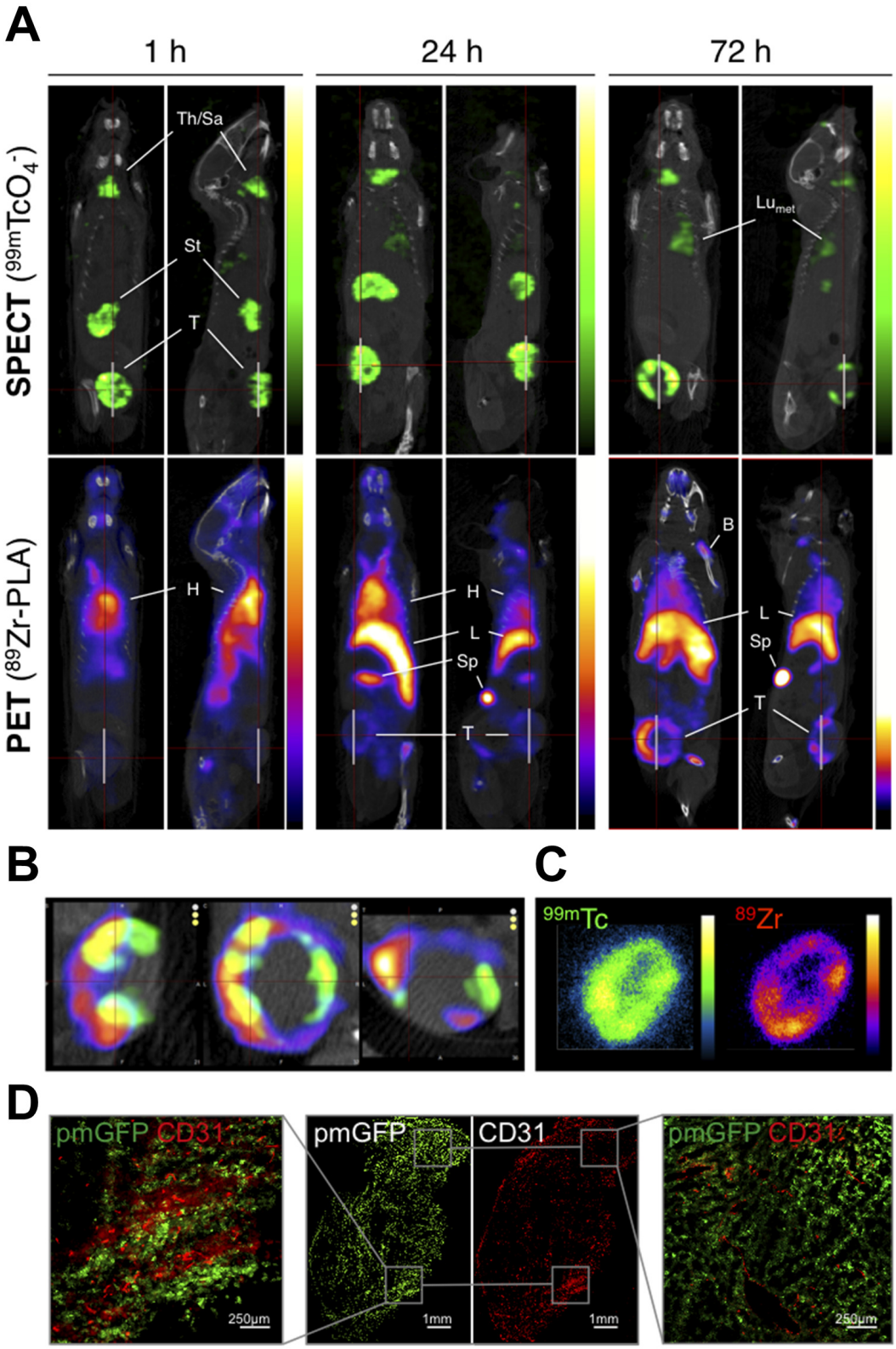

Figure 3. Tracking a nanomedicine to primary and secondary cancer lesions | Liposomal alendronate was radiolabelled with the PET isotope ^{89}Zr (^{89}Zr-PLA) and administered to animals bearing primary breast tumours that had already spontaneously metastasized (as determined by $^{99m}TcO4^-$ -afforded NIS-SPECT/CT). **(A)** Coronal and sagittal SPECT-CT (top; cancer cells) and PET-CT (bottom; nanomedicine) images centred at the tumours of the same animal are shown at indicated time points after intravenous administration of ^{89}Zr-PLA. SPECT-CT images show identical biodistribution over time with high uptake in endogenous NIS-expressing organs (stomach, thyroid) and NIS-FP-expressing cancer cells in the primary tumour (T) and metastases (LN_{met} and Lu_{met}). PET-CT images show the increasing uptake of ^{89}Zr-PLA over time in the primary tumour (T), spleen (Sp), liver (L), and bone (B) and decreasing amounts in the blood pool/heart (H). For corresponding time–activity curves refer to (Edmonds, Volpe, 2016). **(B)** Co-registered SPECT/PET/CT images of the primary tumour (from left to right: sagittal, coronal, transverse) showing a high degree of colocalization but also intra-tumoral heterogeneity of ^{89}Zr-PLA (purple scale); $^{99m}TcO_4^-$ -NIS signals (green scale) show live cancer cells. **(C)** Autoradiography images (left, ^{99m}Tc; right, ^{89}Zr) of a coronal slice from the same tumour as in (B) showing a high degree of colocalization and heterogeneity. **(D)** Fluorescence microscopy of an adjacent slice of the same tumour as in (B/C) showing areas of high and low microvascular density (determined by anti-CD31 staining).

[The figure is reproduced from (Edmonds, Volpe, 2016) (https://pubs.acs.org/doi/10.1021/acsnano.6b05935) with permission from ACS; further permissions related to the material excerpted should be directed to the ACS].

Tab.1 Reporter genes and corresponding imaging tracers and substrates.

Reporter type	Reporter name	Imaging tracer / substrate	Properties	Limitations	Ref.
Cell surface receptor	Human somato-statin receptor type 2 (hSSTr2)	**PET:** ^{68}Ga-DOTATOC, ^{68}Ga-DOTATATE; **SPECT:** ^{111}In-DOTA-BASS; (best tracers selected here).	G-protein-coupled receptor; several tracers cross the BBB.	Endogenous expression in brain, adrenal glands, kidneys, spleen, stomach and many tumours (*i.e.* SCLC, pituitary, endocrine, pancreatic, paraganglioma, medullary thyroid carcinoma, pheochromocytoma); tracers may cause cell signalling and change proliferation.	(Chaudhuri et al., 2001;Rogers et al., 1999;Rogers et al., 2000;Zinn et al., 2000)
Cell surface receptor	Dopamin receptor (D_2R)-	**PET:** [^{18}F]FESP, [^{11}C]Raclopride, [^{11}C]N-methylspiperone.	G-protein-coupled receptor; tracers cross BBB.	Slow clearance of [^{18}F]FESP; high background in the pituitary gland and striatum due to endogenous expression.	(Hwang et al., 2007;Liang et al., 2001;MacLaren et al., 1999;Satyamurthy et al., 1990)
Cell surface receptor	Transferrin receptor (TfR)	**MRI:** Transferrin-conjugated SPIO.		Transferrin-conjugated SPIO particles are internalized by cells ectopically expressing TfR.	(Weissleder et al., 2000)
Cell surface-expressed antigen	Human Carcinoembryonic antigen (hCEA)*	**PET:** ^{124}I-anti-CEA scFv-Fc H310A antibody fragment, [^{18}F]FB-T84.66 diabody; **SPECT:** ^{99m}Tc-anti-CEA Fab' (FDA approved), ^{111}In-ZCE-025, ^{111}In-anti-CEA F023C5i.	Overexpressed in pancreatic, gastric, colorectal and medullary thyroid cancers.	CEA not expressed in healthy adult human cells, except for colon lumen; tracers do not cross BBB.	(Griffin et al., 1991;Hammarstrom, 1999;Hong et al., 2008;Kenanova et al., 2009)
Cell surface protein	Glutamate carboxypeptidase 2* (PSMA)	**PET:** [^{18}F]DCFPyL, [^{18}F]DCFBC; **SPECT:** [^{125}I]DCFPyL; anti-PSMA antibodies can be flexibly labelled, e.g J951-IR800.		Background signal in kidneys; tracers do not cross BBB.	(Castanares et al., 2014)
Transporter	Sodium iodide symporter (NIS) [human, mouse, rat]	**PET:** $^{124}I^-$, [^{18}F]BF_4^-, [^{18}F]SO_3F^-, [^{18}F]PF_6^-; **SPECT:** $^{99m}TcO_4^-$; $^{123}I^-$.	Symports sodium ions.	Endogenously expressed in l\thyroid, stomach, lacrimal, salivary and lactating mammary glands, small intestine, choroid plexus and testicles; tracers do not cross BBB.	(Dai et al., 1996;Jauregui-Osoro et al., 2010;Jiang et al., 2018;Khoshnevisan et al., 2017;Khoshnevisan et al., 2016)
Transporter	Norepinephrin transporter (NET)	**PET:** [^{124}I]MIBG; [^{11}C]hydroxyephedrine; **SPECT:** [^{123}I]MIBG.		Endogenously expressed in organs with sympathetic innervation (heart, brain), tracers do not cross BBB.	(Moroz et al., 2007)
Transporter	Dopamin transporter (DAT)	**PET:** [^{11}C]CFT, [^{11}C]PE2I, [^{18}F]FP-CIT; **SPECT:** ^{123}I-β-CIT, ^{123}I-FP-CIT, ^{123}I-Ioflupane, ^{99m}TRODAT.	NaCl-dependent; tracers cross BBB.	Few data in public domain.	Patent: (Martin Pulé (London), 2015)
Artificial cell surface	Anti-PEG Fab	**PET:** ^{124}I-PEG-SHPP; **MRI:** SPIO-PEG;	Some tracers cross BBB; PEG is non-toxic	Iodine tracers bear risk of deiodination.	(Chuang et al., 2010)

molecule	fragment*	**Fluorescence:** *e.g.* NIR797-PEG.	and FDA approved.		
Artificial protein	Lysine-rich protein	**MRI:** Chemical exchange saturation transfer (CEST).	Frequency-selective contrast.		(Farrar et al., 2015;Gilad et al., 2007)
Enzyme	HSV1-*tk* and mutants-	**PET:** [^{124}I]FIAU, [^{18}F]FEAU, [^{18}F]FHBG.	Kinase causing cellular tracer trapping; suicide gene property.	Tracers do not cross the BBB; high activity in organs involved in clearance.	(Tjuvajev et al., 1995)
Enzyme	hmtk2/hΔTK2	**PET:** [^{124}I]FIAU, [^{18}F]FEAU, [^{18}F]FMAU (hTK2-N93D/L109F).	Kinase causing cellular tracer trapping.	Tracers do not cross the BBB.	(Ponomarev et al., 2007)
Enzyme	hdCK	**PET:** [^{124}I]FIAU, [^{18}F]FEAU.	Kinase causing cellular tracer trapping.	Tracers do not cross the BBB.	(Lee, Zhang, 2017;Likar, Zurita, 2010)
Enzyme	β-galacto-sidase	**PET:** 2-(4-[^{123}I]iodophenyl)ethyl-1-thio-*β-D*-galactopyranoside, 3-(2'-[^{18}F]fluoroethoxy)-2-nitrophenyl-*β-D*-galactopyranoside, 3-[^{11}C]methoxy-2-nitrophenyl-*β-D*-galactopyranoside; **SPECT:** 5-[^{125}I]iodoindol-3-yl-β-D-galactopyranoside; **PAT:** 4-chloro-3-bromoindole-galactose (X-gal); **MRI:** EgadMe.	Glycoside hydrolase.	Cellular toxicity may change with substrates.	(Li et al., 2007;Liu and Mason, 2010;Louie et al., 2000)
Enzyme	Tyrosinase	**PET:** [^{18}F]P3BZA-melanin avid probe; **MRI:** Melanin due to ability to chelate metal ions (Fe^{3+}); **PAT:** Melanin.	Copper-containing enzyme.	Low expression levels; no clinical use.	(Krumholz et al., 2011;Ponomarev, Doubrovin, 2004;Weissleder et al., 1997)
Enzyme	Firefly luciferase	Luciferin and derivatives.	Substrate-dependent, (often: orange/red)	No clinical use.	(Mezzanotte, van 't Root, 2017;Ugarova, 1989)
Enzyme	Renilla luciferase	Coelenterazine	482-547 nm emission	No clinical use.	(Lorenz et al., 1991)
Enzyme	Gaussia luciferase	Coelenterazine	480-600 nm emission	No clinical use.	(Inoue et al., 2011;Tannous, 2009;Tannous et al., 2005)
Enzyme	Green Click Beetle luciferase	Luciferin, naphtyl luciferin.	Emission varies in sub-species: green (548 nm), yellow-green (565 nm), orange (594 nm) and near-infrared.	No clinical use.	(Biggley et al., 1967;Mezzanotte et al., 2014;Mezzanotte et al., 2011;Wood et al., 1989)
Monomeric fluorescent proteins (mFP)	eGFP A206K**		488(ex)/507(em) nm	No clinical use.	(Ormo et al., 1996)
	mCherry**		587/610 nm	No clinical use.	(Shaner et al., 2004)

	TagRFP**		555/584 nm	No clinical use.	(Merzlyak et al., 2007)
	mPlum**		590/649 nm; also used for PAT.	No clinical use.	(Lin et al., 2009)
	mNeptune**		600/650 nm	No clinical use.	(Kremers et al., 2009)
Fluorescent protein	E2-Crimson		611/646 nm	No clinical use, tetramer.	(Liu et al., 2013)
NIR fluorescent proteins	IFP1.4	Exogenously added biliverdin (BV)	684/708 nm	No clinical use; dimer; need for exogenous BV.	(Shcherbakova and Verkhusha, 2013;Shu et al., 2009)
	iRFP 670	Endogenous biliverdin sufficient	643/670 nm; also used for PAT.	No clinical use; dimer.	(Deliolanis et al., 2014;Filonov et al., 2011;Shcherbakova and Verkhusha, 2013)
	iRFP 713	Endogenous biliverdin sufficient	690/713 nm; also used for PAT.	No clinical use; dimer.	(Deliolanis, Ale, 2014;Filonov, Piatkevich, 2011;Shcherbakova and Verkhusha, 2013)
Photoactivatable protein	Kaede**		518/580 nm	No clinical use.	(Ando et al., 2002)
	IrisFP**		516/580 nm	No clinical use.	(Adam et al., 2008)
Photoconvertible protein	Dendra2**		507 nm to 573 nm switch	No clinical use; switch is irreversible.	(Gurskaya et al., 2006)
Iron carrier protein	Ferritin	**MRI:** iron.		Iron is not equally distributed across the brain and therefore may cause local susceptibility shifts that are above the MRI detection limit.	(Cohen et al., 2005;Genove et al., 2005)
Gas-filled protein complex	GvpA/ GvpC	**Ultrasound:** gas vesicles generate contrast.	Reporter gene cluster required.	Not yet validated for use in mammalian cells.	(Raymond W. Bourdeau, 2018)

* Any other modality can be used provided a suitable contrast forming moiety will be attached to PEG and the CEA antibodies, respectively.
**Can be used in fusion with other reporter genes without introduction of artificial protein clustering.

References

Adam V, Lelimousin M, Boehme S, Desfonds G, Nienhaus K, Field MJ, et al. Structural characterization of IrisFP, an optical highlighter undergoing multiple photo-induced transformations. Proc Natl Acad Sci U S A. 2008;105:18343-8.

Alanentalo T, Loren CE, Larefalk A, Sharpe J, Holmberg D, Ahlgren U. High-resolution three-dimensional imaging of islet-infiltrate interactions based on optical projection tomography assessments of the intact adult mouse pancreas. J Biomed Opt. 2008;13:054070.

Alieva M, Ritsma L, Giedt RJ, Weissleder R, van Rheenen J. Imaging windows for long-term intravital imaging: General overview and technical insights. Intravital. 2014;3:e29917.

Ando R, Hama H, Yamamoto-Hino M, Mizuno H, Miyawaki A. An optical marker based on the UV-induced green-to-red photoconversion of a fluorescent protein. Proc Natl Acad Sci U S A. 2002;99:12651-6.

Ariel P. A beginner's guide to tissue clearing. Int J Biochem Cell Biol. 2017;84:35-9.

Arranz A, Dong D, Zhu S, Savakis C, Tian J, Ripoll J. In-vivo optical tomography of small scattering specimens: time-lapse 3D imaging of the head eversion process in Drosophila melanogaster. Sci Rep. 2014;4:7325.

Bassi A, Fieramonti L, D'Andrea C, Mione M, Valentini G. In vivo label-free three-dimensional imaging of zebrafish vasculature with optical projection tomography. J Biomed Opt. 2011;16:100502.

Basu S, Hess S, Nielsen Braad PE, Olsen BB, Inglev S, Hoilund-Carlsen PF. The Basic Principles of FDG-PET/CT Imaging. PET Clin. 2014;9:355-70, v.

Bianchi A, Dufort S, Lux F, Fortin PY, Tassali N, Tillement O, et al. Targeting and in vivo imaging of non-small-cell lung cancer using nebulized multimodal contrast agents. Proc Natl Acad Sci U S A. 2014;111:9247-52.

Biggley WH, Lloyd JE, Seliger HH. The Spectral Distribution of Firefly Light. II. The Journal of General Physiology. 1967;50:1681-92.

Boardman DA, Philippeos C, Fruhwirth GO, Ibrahim MAA, Hannen RF, Cooper D, et al. Expression of a Chimeric Antigen Receptor Specific for Donor HLA Class I Enhances the Potency of Human Regulatory T Cells in Preventing Human Skin Transplant Rejection. American Journal of Transplantation. 2017:n/a-n/a.

Bressan RB, Dewari PS, Kalantzaki M, Gangoso E, Matjusaitis M, Garcia-Diaz C, et al. Efficient CRISPR/Cas9-assisted gene targeting enables rapid and precise genetic manipulation of mammalian neural stem cells. Development. 2017;144:635-48.

Carlson SK, Classic KL, Hadac EM, Dingli D, Bender CE, Kemp BJ, et al. Quantitative molecular imaging of viral therapy for pancreatic cancer using an engineered measles virus expressing the sodium-iodide symporter reporter gene. AJR American journal of roentgenology. 2009;192:279-87.

Castanares MA, Mukherjee A, Chowdhury WH, Liu M, Chen Y, Mease RC, et al. Evaluation of Prostate-Specific Membrane Antigen as an Imaging Reporter. J Nucl Med. 2014;55:805-11.

Catana C. Principles of Simultaneous PET/MR Imaging. Magn Reson Imaging Clin N Am. 2017;25:231-43.

Chaudhuri TR, Rogers BE, Buchsbaum DJ, Mountz JM, Zinn KR. A noninvasive reporter system to image adenoviral-mediated gene transfer to ovarian cancer xenografts. Gynecologic oncology. 2001;83:432-8.

Che J, Doubrovin M, Serganova I, Ageyeva L, Zanzonico P, Blasberg R. hNIS-IRES-eGFP dual reporter gene imaging. Mol Imaging. 2005;4:128-36.

Cheddad A, Svensson C, Sharpe J, Georgsson F, Ahlgren U. Image Processing Assisted Algorithms for Optical Projection Tomography. IEEE Transactions on Medical Imaging. 2012;31:1-15.

Cheng SH, Yu D, Tsai HM, Morshed RA, Kanojia D, Lo LW, et al. Dynamic In Vivo SPECT Imaging of Neural Stem Cells Functionalized with Radiolabeled Nanoparticles for Tracking of Glioblastoma. J Nucl Med. 2016;57:279-84.

Chuang KH, Wang HE, Cheng TC, Tzou SC, Tseng WL, Hung WC, et al. Development of a universal anti-polyethylene glycol reporter gene for noninvasive imaging of PEGylated probes. J Nucl Med. 2010;51:933-41.

Ciarrocchi E, Belcari N. Cerenkov luminescence imaging: physics principles and potential applications in biomedical sciences. EJNMMI Phys. 2017;4:14.

Cohen B, Dafni H, Meir G, Harmelin A, Neeman M. Ferritin as an Endogenous MRI Reporter for Noninvasive Imaging of Gene Expression in C6 Glioma Tumors. Neoplasia. 2005;7:109-17.

Condeelis J, Segall JE. Intravital imaging of cell movement in tumours. Nat Rev Cancer. 2003;3:921-30.

Dai G, Levy O, Carrasco N. Cloning and characterization of the thyroid iodide transporter. Nature. 1996;379:458-60.

Dean-Ben XL, Gottschalk S, Mc Larney B, Shoham S, Razansky D. Advanced optoacoustic methods for multiscale imaging of in vivo dynamics. Chem Soc Rev. 2017;46:2158-98.

Deleye S, Van Holen R, Verhaeghe J, Vandenberghe S, Stroobants S, Staelens S. Performance evaluation of small-animal multipinhole muSPECT scanners for mouse imaging. European journal of nuclear medicine and molecular imaging. 2013;40:744-58.

Deliolanis NC, Ale A, Morscher S, Burton NC, Schaefer K, Radrich K, et al. Deep-tissue reporter-gene imaging with fluorescence and optoacoustic tomography: a performance overview. Mol Imaging Biol. 2014;16:652-60.

Dingli D, Kemp BJ, O'Connor MK, Morris JC, Russell SJ, Lowe VJ. Combined I-124 positron emission tomography/computed tomography imaging of NIS gene expression in animal models of stably transfected and intravenously transfected tumor. Mol Imaging Biol. 2006;8:16-23.

Diocou S, Volpe A, Jauregui-Osoro M, Boudjemeline M, Chuamsaamarkkee K, Man F, et al. [18F]tetrafluoroborate-PET/CT enables sensitive tumor and metastasis in vivo imaging in a sodium iodide symporter-expressing tumor model. Scientific Reports. 2017;7:946.

Diot G, Metz S, Noske A, Liapis E, Schroeder B, Ovsepian SV, et al. Multispectral Optoacoustic Tomography (MSOT) of Human Breast Cancer. Clinical Cancer Research. 2017;23:6912.

Dohan O, De la Vieja A, Paroder V, Riedel C, Artani M, Reed M, et al. The sodium/iodide Symporter (NIS): characterization, regulation, and medical significance. Endocr Rev. 2003;24:48-77.

Dunlap P. Biochemistry and genetics of bacterial bioluminescence. Adv Biochem Eng Biotechnol. 2014;144:37-64.

Edmonds S, Volpe A, Shmeeda H, Parente-Pereira AC, Radia R, Baguna-Torres J, et al. Exploiting the Metal-Chelating Properties of the Drug Cargo for In Vivo Positron Emission Tomography Imaging of Liposomal Nanomedicines. ACS Nano. 2016;10:10294-307.

Ellison GM, Vicinanza C, Smith AJ, Aquila I, Leone A, Waring CD, et al. Adult c-kit(pos) cardiac stem cells are necessary and sufficient for functional cardiac regeneration and repair. Cell. 2013;154:827-42.

Entenberg D, Pastoriza JM, Oktay MH, Voiculescu S, Wang Y, Sosa MS, et al. Time-lapsed, large-volume, high-resolution intravital imaging for tissue-wide analysis of single cell dynamics. Methods. 2017;128:65-77.

Entenberg D, Voiculescu S, Guo P, Borriello L, Wang Y, Karagiannis GS, et al. A permanent window for the murine lung enables high-resolution imaging of cancer metastasis. Nat Methods. 2018;15:73-80.

Farrar CT, Buhrman JS, Liu G, Kleijn A, Lamfers ML, McMahon MT, et al. Establishing the Lysine-rich Protein CEST Reporter Gene as a CEST MR Imaging Detector for Oncolytic Virotherapy. Radiology. 2015;275:746-54.

Filonov GS, Piatkevich KD, Ting LM, Zhang J, Kim K, Verkhusha VV. Bright and stable near-infrared fluorescent protein for in vivo imaging. Nat Biotechnol. 2011;29:757-61.

Fruhwirth GO, Diocou S, Blower PJ, Ng T, Mullen GE. A whole-body dual-modality radionuclide optical strategy for preclinical imaging of metastasis and heterogeneous treatment response in different microenvironments. J Nucl Med. 2014;55:686-94.

Galon J, Mlecnik B, Bindea G, Angell HK, Berger A, Lagorce C, et al. Towards the introduction of the 'Immunoscore' in the classification of malignant tumours. J Pathol. 2014;232:199-209.

Genove G, DeMarco U, Xu H, Goins WF, Ahrens ET. A new transgene reporter for in vivo magnetic resonance imaging. Nat Med. 2005;11:450-4.

Gilad AA, McMahon MT, Walczak P, Winnard PT, Jr., Raman V, van Laarhoven HW, et al. Artificial reporter gene providing MRI contrast based on proton exchange. Nat Biotechnol. 2007;25:217-9.

Gleave JA, Wong MD, Dazai J, Altaf M, Henkelman RM, Lerch JP, et al. Neuroanatomical phenotyping of the mouse brain with three-dimensional autofluorescence imaging. Physiol Genomics. 2012;44:778-85.

Graves EE, Weissleder R, Ntziachristos V. Fluorescence molecular imaging of small animal tumor models. Curr Mol Med. 2004;4:419-30.

Griffin TW, Brill AB, Stevens S, Collins JA, Bokhari F, Bushe H, et al. Initial clinical study of indium-111-labeled clone 110 anticarcinoembryonic antigen antibody in patients with colorectal cancer. Journal of clinical oncology : official journal of the American Society of Clinical Oncology. 1991;9:631-40.

Groot-Wassink T, Aboagye EO, Wang Y, Lemoine NR, Keith WN, Vassaux G. Noninvasive imaging of the transcriptional activities of human telomerase promoter fragments in mice. Cancer Res. 2004;64:4906-11.

Gupta S, Utoft R, Hasseldam H, Schmidt-Christensen A, Hannibal TD, Hansen L, et al. Global and 3D spatial assessment of neuroinflammation in rodent models of Multiple Sclerosis. PLoS One. 2013;8:e76330.

Gurskaya NG, Verkhusha VV, Shcheglov AS, Staroverov DB, Chepurnykh TV, Fradkov AF, et al. Engineering of a monomeric green-to-red photoactivatable fluorescent protein induced by blue light. Nat Biotechnol. 2006;24:461-5.

Hammarstrom S. The carcinoembryonic antigen (CEA) family: structures, suggested functions and expression in normal and malignant tissues. Seminars in cancer biology. 1999;9:67-81.

Hekman MCH, Rijpkema M, Bos DL, Oosterwijk E, Goldenberg DM, Mulders PFA, et al. Detection of Micrometastases Using SPECT/Fluorescence Dual-Modality Imaging in a CEA-Expressing Tumor Model. J Nucl Med. 2017;58:706-10.

Higuchi T, Anton M, Saraste A, Dumler K, Pelisek J, Nekolla SG, et al. Reporter gene PET for monitoring survival of transplanted endothelial progenitor cells in the rat heart after pretreatment with VEGF and atorvastatin. J Nucl Med. 2009;50:1881-6.

Hong H, Sun J, Cai W. Radionuclide-Based Cancer Imaging Targeting the Carcinoembryonic Antigen. Biomarker Insights. 2008;3:435-51.

Hwang DW, Kang JH, Chang YS, Jeong JM, Chung JK, Lee MC, et al. Development of a dual membrane protein reporter system using sodium iodide symporter and mutant dopamine D2 receptor transgenes. J Nucl Med. 2007;48:588-95.

Inoue Y, Sheng F, Kiryu S, Watanabe M, Ratanakanit H, Izawa K, et al. Gaussia luciferase for bioluminescence tumor monitoring in comparison with firefly luciferase. Mol Imaging. 2011;10:377-85.

Jauregui-Osoro M, Sunassee K, Weeks AJ, Berry DJ, Paul RL, Cleij M, et al. Synthesis and biological evaluation of [F-18]tetrafluoroborate: a PET imaging agent for thyroid disease and reporter gene imaging of the sodium/iodide symporter. European journal of nuclear medicine and molecular imaging. 2010;37:2108-16.

Jiang H, Bansal A, Goyal R, Peng K-W, Russell SJ, DeGrado TR. Synthesis and evaluation of 18F-hexafluorophosphate as a novel PET probe for imaging of sodium/iodide symporter in a murine C6-glioma tumor model. Bioorganic & Medicinal Chemistry. 2018;26:225-31.

Jiang T, Du L, Li M. Lighting up bioluminescence with coelenterazine: strategies and applications. Photochem Photobiol Sci. 2016;15:466-80.

Jost SC, Collins L, Travers S, Piwnica-Worms D, Garbow JR. Measuring brain tumor growth: combined bioluminescence imaging-magnetic resonance imaging strategy. Mol Imaging. 2009;8:245-53.

Jung W, Kim J, Jeon M, Chaney EJ, Stewart CN, Boppart SA. Handheld optical coherence tomography scanner for primary care diagnostics. IEEE Trans Biomed Eng. 2011;58:741-4.

Karagiannis ED, Boyden ES. Expansion microscopy: development and neuroscience applications. Curr Opin Neurobiol. 2018;50:56-63.

Kenanova V, Barat B, Olafsen T, Chatziioannou A, Herschman HR, Braun J, et al. Recombinant carcinoembryonic antigen as a reporter gene for molecular imaging. European journal of nuclear medicine and molecular imaging. 2009;36:104-14.

Keu KV, Witney TH, Yaghoubi S, Rosenberg J, Kurien A, Magnusson R, et al. Reporter gene imaging of targeted T cell immunotherapy in recurrent glioma. Sci Transl Med. 2017;9.

Khoshnevisan A, Chuamsaamarkkee K, Boudjemeline M, Jackson A, Smith GE, Gee AD, et al. 18F-Fluorosulfate for PET Imaging of the Sodium-Iodide Symporter: Synthesis and Biologic Evaluation In Vitro and In Vivo. J Nucl Med. 2017;58:156-61.

Khoshnevisan A, Jauregui-Osoro M, Shaw K, Torres JB, Young JD, Ramakrishnan NK, et al. [(18)F]tetrafluoroborate as a PET tracer for the sodium/iodide symporter: the importance of specific activity. EJNMMI Res. 2016;6:34.

Kircher MF, Gambhir SS, Grimm J. Noninvasive cell-tracking methods. Nat Rev Clin Oncol. 2011;8:677-88.

Knieling F, Neufert C, Hartmann A, Claussen J, Urich A, Egger C, et al. Multispectral Optoacoustic Tomography for Assessment of Crohn's Disease Activity. N Engl J Med. 2017;376:1292-4.

Kogai T, Brent GA. The sodium iodide symporter (NIS): regulation and approaches to targeting for cancer therapeutics. Pharmacol Ther. 2012;135:355-70.

Kokoris MS, Black ME. Characterization of herpes simplex virus type 1 thymidine kinase mutants engineered for improved ganciclovir or acyclovir activity. Protein Sci. 2002;11:2267-72.

Koya RC, Mok S, Comin-Anduix B, Chodon T, Radu CG, Nishimura MI, et al. Kinetic phases of distribution and tumor targeting by T cell receptor engineered lymphocytes inducing robust antitumor responses. Proc Natl Acad Sci U S A. 2010;107:14286-91.

Kremers GJ, Hazelwood KL, Murphy CS, Davidson MW, Piston DW. Photoconversion in orange and red fluorescent proteins. Nat Methods. 2009;6:355-8.

Krumholz A, VanVickle-Chavez SJ, Yao J, Fleming TP, Gillanders WE, Wang LV. Photoacoustic microscopy of tyrosinase reporter gene in vivo. J Biomed Opt. 2011;16.

Lajtos I, Czernin J, Dahlbom M, Daver F, Emri M, Farshchi-Heydari S, et al. Cold wall effect eliminating method to determine the contrast recovery coefficient for small animal PET scanners using the NEMA NU-4 image quality phantom. Physics in medicine and biology. 2014;59:2727-46.

Lavoue V, Cabillic F, Toutirais O, Thedrez A, Dessarthe B, de La Pintiere CT, et al. Sensitization of ovarian carcinoma cells with zoledronate restores the cytotoxic capacity of Vgamma9Vdelta2 T cells impaired by the prostaglandin E2 immunosuppressive factor: implications for immunotherapy. Int J Cancer. 2012;131:E449-62.

Lee JT, Zhang H, Moroz MA, Likar Y, Shenker L, Sumzin N, et al. Comparative Analysis of Human Nucleoside Kinase-Based Reporter Systems for PET Imaging. Mol Imaging Biol. 2017;19:100-8.

Li J, Chen L, Du L, Li M. Cage the firefly luciferin! - a strategy for developing bioluminescent probes. Chem Soc Rev. 2013;42:662-76.

Li L, Zemp RJ, Lungu G, Stoica G, Wang LV. Photoacoustic imaging of lacZ gene expression in vivo. J Biomed Opt. 2007;12:020504.

Lian L, Deng Y, Xie W, Xu G, Yang X, Zhang Z, et al. Enhancement of the localization and quantitative performance of fluorescence molecular tomography by using linear nBorn method. Opt Express. 2017;25:2063-79.

Liang Q, Satyamurthy N, Barrio JR, Toyokuni T, Phelps MP, Gambhir SS, et al. Noninvasive, quantitative imaging in living animals of a mutant dopamine D2 receptor reporter gene in which ligand binding is uncoupled from signal transduction. Gene therapy. 2001;8:1490-8.

Likar Y, Zurita J, Dobrenkov K, Shenker L, Cai S, Neschadim A, et al. A new pyrimidine-specific reporter gene: a mutated human deoxycytidine kinase suitable for PET during treatment with acycloguanosine-based cytotoxic drugs. J Nucl Med. 2010;51:1395-403.

Lin MZ, McKeown MR, Ng HL, Aguilera TA, Shaner NC, Campbell RE, et al. Autofluorescent proteins with excitation in the optical window for intravital imaging in mammals. Chemistry & biology. 2009;16:1169.

Linette GP, Stadtmauer EA, Maus MV, Rapoport AP, Levine BL, Emery L, et al. Cardiovascular toxicity and titin cross-reactivity of affinity-enhanced T cells in myeloma and melanoma. Blood. 2013;122:863-71.

Liu L, Mason RP. Imaging β-Galactosidase Activity in Human Tumor Xenografts and Transgenic Mice Using a Chemiluminescent Substrate. PLoS One. 2010;5.

Liu M, Schmitner N, Sandrian MG, Zabihian B, Hermann B, Salvenmoser W, et al. In vivo three dimensional dual wavelength photoacoustic tomography imaging of the far red fluorescent protein E2-Crimson expressed in adult zebrafish. Biomed Opt Express. 2013;4:1846-55.

Lorenz WW, McCann RO, Longiaru M, Cormier MJ. Isolation and expression of a cDNA encoding Renilla reniformis luciferase. Proc Natl Acad Sci U S A. 1991;88:4438-42.

Louie AY, Huber MM, Ahrens ET, Rothbacher U, Moats R, Jacobs RE, et al. In vivo visualization of gene expression using magnetic resonance imaging. Nat Biotechnol. 2000;18:321-5.

Ma R, Taruttis A, Ntziachristos V, Razansky D. Multispectral optoacoustic tomography (MSOT) scanner for whole-body small animal imaging. Opt Express. 2009;17:21414-26.

MacLaren DC, Gambhir SS, Satyamurthy N, Barrio JR, Sharfstein S, Toyokuni T, et al. Repetitive, non-invasive imaging of the dopamine D2 receptor as a reporter gene in living animals. Gene therapy. 1999;6:785-91.

Makela AV, Foster PJ. Imaging macrophage distribution and density in mammary tumors and lung metastases using fluorine-19 MRI cell tracking. Magn Reson Med. 2018.

Man F, Lim L, Shmeeda H, Gabizon A, Blower P, Fruhwirth G, et al. Direct Cell Labelling with 89Zr(oxine)4 allows In Vivo PET Imaging of Gamma-delta T-cells in a Breast Cancer Model. Journal of Nuclear Medicine. 2017;58:185.

Mankoff DA. A definition of molecular imaging. J Nucl Med. 2007;48:18N, 21N.

Mansfield JR, Hoyt C, Levenson RM. Visualization of microscopy-based spectral imaging data from multi-label tissue sections. Curr Protoc Mol Biol. 2008;Chapter 14:Unit 14 9.

Martin Pulé (London) ABL, Louise Kiru (London), Mark Lythgoe (London), Adrien Peters (Brighton) Detecting a Therapeutic Cell. Publication number: 20170056534. 2015.

Mattarollo SR, Kenna T, Nieda M, Nicol AJ. Chemotherapy and zoledronate sensitize solid tumour cells to Vgamma9Vdelta2 T cell cytotoxicity. Cancer Immunol Immunother. 2007;56:1285-97.

Maude SL, Laetsch TW, Buechner J, Rives S, Boyer M, Bittencourt H, et al. Tisagenlecleucel in Children and Young Adults with B-Cell Lymphoblastic Leukemia. N Engl J Med. 2018;378:439-48.

McCann CM, Waterman P, Figueiredo JL, Aikawa E, Weissleder R, Chen JW. Combined magnetic resonance and fluorescence imaging of the living mouse brain reveals glioma response to chemotherapy. Neuroimage. 2009;45:360-9.

McGinty J, Taylor HB, Chen L, Bugeon L, Lamb JR, Dallman MJ, et al. In vivo fluorescence lifetime optical projection tomography. Biomed Opt Express. 2011;2:1340-50.

McNally LR, Mezera M, Morgan DE, Frederick PJ, Yang ES, Eltoum IE, et al. Current and Emerging Clinical Applications of Multispectral Optoacoustic Tomography (MSOT) in Oncology. Clin Cancer Res. 2016;22:3432-9.

Merron A, Peerlinck I, Martin-Duque P, Burnet J, Quintanilla M, Mather S, et al. SPECT/CT imaging of oncolytic adenovirus propagation in tumours in vivo using the Na/I symporter as a reporter gene. Gene therapy. 2007;14:1731-8.

Merzlyak EM, Goedhart J, Shcherbo D, Bulina ME, Shcheglov AS, Fradkov AF, et al. Bright monomeric red fluorescent protein with an extended fluorescence lifetime. Nat Methods. 2007;4:555-7.

Mezzanotte L, An N, Mol IM, Lowik CW, Kaijzel EL. A new multicolor bioluminescence imaging platform to investigate NF-kappaB activity and apoptosis in human breast cancer cells. PLoS One. 2014;9:e85550.

Mezzanotte L, Que I, Kaijzel E, Branchini B, Roda A, Lowik C. Sensitive dual color in vivo bioluminescence imaging using a new red codon optimized firefly luciferase and a green click beetle luciferase. PLoS One. 2011;6:e19277.

Mezzanotte L, van 't Root M, Karatas H, Goun EA, Lowik C. In Vivo Molecular Bioluminescence Imaging: New Tools and Applications. Trends Biotechnol. 2017;35:640-52.

Minn AJ, Kang Y, Serganova I, Gupta GP, Giri DD, Doubrovin M, et al. Distinct organ-specific metastatic potential of individual breast cancer cells and primary tumors. J Clin Invest. 2005;115:44-55.

Mogensen M, Thrane L, Jorgensen TM, Andersen PE, Jemec GB. OCT imaging of skin cancer and other dermatological diseases. J Biophotonics. 2009;2:442-51.

Moroz MA, Serganova I, Zanzonico P, Ageyeva L, Beresten T, Dyomina E, et al. Imaging hNET reporter gene expression with 124I-MIBG. J Nucl Med. 2007;48:827-36.

Moroz MA, Zhang H, Lee J, Moroz E, Zurita J, Shenker L, et al. Comparative Analysis of T Cell Imaging with Human Nuclear Reporter Genes. J Nucl Med. 2015;56:1055-60.

Nagy K, Toth M, Major P, Patay G, Egri G, Haggkvist J, et al. Performance evaluation of the small-animal nanoScan PET/MRI system. J Nucl Med. 2013;54:1825-32.

Neelapu SS, Locke FL, Bartlett NL, Lekakis LJ, Miklos DB, Jacobson CA, et al. Axicabtagene Ciloleucel CAR T-Cell Therapy in Refractory Large B-Cell Lymphoma. N Engl J Med. 2017;377:2531-44.

Ntziachristos V. Fluorescence molecular imaging. Annu Rev Biomed Eng. 2006;8:1-33.

Ntziachristos V, Razansky D. Molecular imaging by means of multispectral optoacoustic tomography (MSOT). Chem Rev. 2010;110:2783-94.

Ntziachristos V, Ripoll J, Wang LV, Weissleder R. Looking and listening to light: the evolution of whole-body photonic imaging. Nat Biotechnol. 2005;23:313-20.

O'Connor JP, Aboagye EO, Adams JE, Aerts HJ, Barrington SF, Beer AJ, et al. Imaging biomarker roadmap for cancer studies. Nat Rev Clin Oncol. 2017;14:169-86.

Oldham M, Sakhalkar H, Wang YM, Guo P, Oliver T, Bentley R, et al. Three-dimensional imaging of whole rodent organs using optical computed and emission tomography. J Biomed Opt. 2007;12:014009.

Oliveira JM, Gomes C, Faria DB, Vieira TS, Silva FA, Vale J, et al. (68)Ga-prostate-specific Membrane Antigen Positron Emission Tomography/Computed Tomography for Prostate Cancer Imaging: A Narrative Literature Review. World J Nucl Med. 2017;16:3-7.

Olsen J, Themstrup L, Jemec GB. Optical coherence tomography in dermatology. G Ital Dermatol Venereol. 2015;150:603-15.

Omar M, Schwarz M, Soliman D, Symvoulidis P, Ntziachristos V. Pushing the optical imaging limits of cancer with multi-frequency-band raster-scan optoacoustic mesoscopy (RSOM). Neoplasia. 2015;17:208-14.

Ormo M, Cubitt AB, Kallio K, Gross LA, Tsien RY, Remington SJ. Crystal structure of the Aequorea victoria green fluorescent protein. Science. 1996;273:1392-5.

Parente-Pereira AC, Shmeeda H, Whilding LM, Zambirinis CP, Foster J, van der Stegen SJ, et al. Adoptive immunotherapy of epithelial ovarian cancer with Vgamma9Vdelta2 T cells, potentiated by liposomal alendronic acid. J Immunol. 2014;193:5557-66.

Perera M, Papa N, Christidis D, Wetherell D, Hofman MS, Murphy DG, et al. Sensitivity, Specificity, and Predictors of Positive (68)Ga-Prostate-specific Membrane Antigen Positron Emission Tomography in Advanced Prostate Cancer: A Systematic Review and Meta-analysis. Eur Urol. 2016;70:926-37.

Pittet MJ, Weissleder R. Intravital imaging. Cell. 2011;147:983-91.

Ponomarev V, Doubrovin M, Serganova I, Vider J, Shavrin A, Beresten T, et al. A novel triple-modality reporter gene for whole-body fluorescent, bioluminescent, and nuclear noninvasive imaging. European journal of nuclear medicine and molecular imaging. 2004;31:740-51.

Ponomarev V, Doubrovin M, Shavrin A, Serganova I, Beresten T, Ageyeva L, et al. A human-derived reporter gene for noninvasive imaging in humans: mitochondrial thymidine kinase type 2. J Nucl Med. 2007;48:819-26.

Portulano C, Paroder-Belenitsky M, Carrasco N. The Na+/I- symporter (NIS): mechanism and medical impact. Endocr Rev. 2014;35:106-49.

Rashid T, Takebe T, Nakauchi H. Novel strategies for liver therapy using stem cells. Gut. 2015;64:1-4.

Ray P, De A, Min JJ, Tsien RY, Gambhir SS. Imaging tri-fusion multimodality reporter gene expression in living subjects. Cancer Res. 2004;64:1323-30.

Raymond W. Bourdeau AL-G, Anupama Lakshmanan, Arash Farhadi, Sripriya Ravindra Kumar, Suchita P. Nety & Mikhail G. Shapiro. Acoustic reporter genes for noninvasive imaging of microorganisms in mammalian hosts. Nature. 2018;553:86-90.

Rodriguez EA, Campbell RE, Lin JY, Lin MZ, Miyawaki A, Palmer AE, et al. The Growing and Glowing Toolbox of Fluorescent and Photoactive Proteins. Trends Biochem Sci. 2017;42:111-29.

Rogers BE, McLean SF, Kirkman RL, Della Manna D, Bright SJ, Olsen CC, et al. In vivo localization of [(111)In]-DTPA-D-Phe1-octreotide to human ovarian tumor xenografts induced to express the somatostatin receptor subtype 2 using an adenoviral vector. Clin Cancer Res. 1999;5:383-93.

Rogers BE, Zinn KR, Buchsbaum DJ. Gene transfer strategies for improving radiolabeled peptide imaging and therapy. The quarterly journal of nuclear medicine : official publication of the Italian Association of Nuclear Medicine (AIMN) [and] the International Association of Radiopharmacology (IAR). 2000;44:208-23.

Satyamurthy N, Barrio JR, Bida GT, Huang SC, Mazziotta JC, Phelps ME. 3-(2'-[18F]fluoroethyl)spiperone, a potent dopamine antagonist: synthesis, structural analysis and in-vivo utilization in humans. International journal of radiation applications and instrumentation Part A, Applied radiation and isotopes. 1990;41:113-29.

Saudemont A, Jespers L, Clay T. Current Status of Gene Engineering Cell Therapeutics. Front Immunol. 2018;9:153.

Schuster SJ, Svoboda J, Chong EA, Nasta SD, Mato AR, Anak O, et al. Chimeric Antigen Receptor T Cells in Refractory B-Cell Lymphomas. N Engl J Med. 2017;377:2545-54.

Shaner NC, Campbell RE, Steinbach PA, Giepmans BN, Palmer AE, Tsien RY. Improved monomeric red, orange and yellow fluorescent proteins derived from Discosoma sp. red fluorescent protein. Nat Biotechnol. 2004;22:1567-72.

Sharpe J, Ahlgren U, Perry P, Hill B, Ross A, Hecksher-Sorensen J, et al. Optical projection tomography as a tool for 3D microscopy and gene expression studies. Science. 2002;296:541-5.

Shcherbakova DM, Verkhusha VV. Near-infrared fluorescent proteins for multicolor in vivo imaging. Nat Methods. 2013;10:751-4.

Shu X, Royant A, Lin MZ, Aguilera TA, Lev-Ram V, Steinbach PA, et al. Mammalian expression of infrared fluorescent proteins engineered from a bacterial phytochrome. Science. 2009;324:804-7.

Sieger S, Jiang S, Schonsiegel F, Eskerski H, Kubler W, Altmann A, et al. Tumour-specific activation of the sodium/iodide symporter gene under control of the glucose transporter gene 1 promoter (GTI-1.3). European journal of nuclear medicine and molecular imaging. 2003;30:748-56.

Song HT, Jordan EK, Lewis BK, Liu W, Ganjei J, Klaunberg B, et al. Rat model of metastatic breast cancer monitored by MRI at 3 tesla and bioluminescence imaging with histological correlation. J Transl Med. 2009;7:88.

Stack EC, Wang C, Roman KA, Hoyt CC. Multiplexed immunohistochemistry, imaging, and quantitation: a review, with an assessment of Tyramide signal amplification, multispectral imaging and multiplex analysis. Methods. 2014;70:46-58.

Swirski FK, Berger CR, Figueiredo JL, Mempel TR, von Andrian UH, Pittet MJ, et al. A near-infrared cell tracker reagent for multiscopic in vivo imaging and quantification of leukocyte immune responses. PLoS One. 2007;2:e1075.

Tannous BA. Gaussia luciferase reporter assay for monitoring biological processes in culture and in vivo. Nature protocols. 2009;4:582-91.

Tannous BA, Kim DE, Fernandez JL, Weissleder R, Breakefield XO. Codon-optimized Gaussia luciferase cDNA for mammalian gene expression in culture and in vivo. Mol Ther. 2005;11:435-43.

Tao A, Shao Y, Zhong J, Jiang H, Shen M, Wang J. Versatile optical coherence tomography for imaging the human eye. Biomed Opt Express. 2013;4:1031-44.

Terrovitis J, Kwok KF, Lautamaki R, Engles JM, Barth AS, Kizana E, et al. Ectopic expression of the sodium-iodide symporter enables imaging of transplanted cardiac stem cells in vivo by single-photon emission computed tomography or positron emission tomography. J Am Coll Cardiol. 2008;52:1652-60.

Tiernan JP, Perry SL, Verghese ET, West NP, Yeluri S, Jayne DG, et al. Carcinoembryonic antigen is the preferred biomarker for in vivo colorectal cancer targeting. Br J Cancer. 2013;108:662-7.

Tjuvajev JG, Stockhammer G, Desai R, Uehara H, Watanabe K, Gansbacher B, et al. Imaging the expression of transfected genes in vivo. Cancer Res. 1995;55:6126-32.

Tsao H, Chin L, Garraway LA, Fisher DE. Melanoma: from mutations to medicine. Genes Dev. 2012;26:1131-55.

Ugarova NN. Luciferase of Luciola mingrelica fireflies. Kinetics and regulation mechanism. Journal of bioluminescence and chemiluminescence. 1989;4:406-18.

USFood&DrugAdministration. FDA approval brings first gene therapy to the United States. 2017a.

USFood&DrugAdministration. FDA approves CAR-T cell therapy to treat adults with certain types of large B-cell lymphoma. 2017b.

Valluru KS, Wilson KE, Willmann JK. Photoacoustic Imaging in Oncology: Translational Preclinical and Early Clinical Experience. Radiology. 2016;280:332-49.

Venugopal V, Chen J, Lesage F, Intes X. Full-field time-resolved fluorescence tomography of small animals. Opt Lett. 2010;35:3189-91.

Vinegoni C, Pitsouli C, Razansky D, Perrimon N, Ntziachristos V. In vivo imaging of Drosophila melanogaster pupae with mesoscopic fluorescence tomography. Nat Methods. 2008;5:45-7.

Volpe A, Man F, Lim L, Khoshnevisan A, Blower JE, Blower PJ, et al. Radionuclide-fluorescence reporter gene imaging to track tumor progression in rodent tumor models. Journal of Visualized Experiments. 2018:e57088.

Wang K, Wang Q, Luo Q, Yang X. Fluorescence molecular tomography in the second near-infrared window. Opt Express. 2015;23:12669-79.

Wang LV, Yao J. A practical guide to photoacoustic tomography in the life sciences. Nat Methods. 2016;13:627-38.

Weissleder R, Moore A, Mahmood U, Bhorade R, Benveniste H, Chiocca EA, et al. In vivo magnetic resonance imaging of transgene expression. Nat Med. 2000;6:351-5.

Weissleder R, Simonova M, Bogdanova A, Bredow S, Enochs WS, Bogdanov A, Jr. MR imaging and scintigraphy of gene expression through melanin induction. Radiology. 1997;204:425-9.

Whitehead LW, McArthur K, Geoghegan ND, Rogers KL. The reinvention of twentieth century microscopy for three-dimensional imaging. Immunol Cell Biol. 2017;95:520-4.

Witney TH, Kettunen MI, Day SE, Hu DE, Neves AA, Gallagher FA, et al. A comparison between radiolabeled fluorodeoxyglucose uptake and hyperpolarized (13)C-labeled pyruvate utilization as methods for detecting tumor response to treatment. Neoplasia. 2009;11:574-82, 1 p following 82.

Wood KV, Lam YA, Seliger HH, McElroy WD. Complementary DNA coding click beetle luciferases can elicit bioluminescence of different colors. Science. 1989;244:700-2.

Zabow G, Dodd S, Moreland J, Koretsky A. Micro-engineered local field control for high-sensitivity multispectral MRI. Nature. 2008;453:1058.

Zacharakis G, Favicchio R, Simantiraki M, Ripoll J. Spectroscopic detection improves multi-color quantification in fluorescence tomography. Biomed Opt Express. 2011;2:431-9.

Zhang H, Qiao H, Bakken A, Gao F, Huang B, Liu YY, et al. Utility of dual-modality bioluminescence and MRI in monitoring stem cell survival and impact on post myocardial infarct remodeling. Acad Radiol. 2011;18:3-12.

Zinn KR, Buchsbaum DJ, Chaudhuri TR, Mountz JM, Grizzle WE, Rogers BE. Noninvasive monitoring of gene transfer using a reporter receptor imaged with a high-affinity peptide radiolabeled with 99mTc or 188Re. J Nucl Med. 2000;41:887-95.